Biogeosciences Discuss., 11, 2305–2342, 2014
www.biogeosciences-discuss.net/11/2305/2014/
doi:10.5194/bgd-11-2305-2014

Biogeosciences Discussions
Open Access

Evaluating remote sensing of deciduous forest phenology at multiple spatial scales using PhenoCam imagery

S. T. Klosterman[1], K. Hufkens[2,1], J. M. Gray[3], E. Melaas[3], O. Sonnentag[1,4], I. Lavine[5], L. Mitchell[6], R. Norman[7], M. A. Friedl[3], and A. D. Richardson[1]

[1]Department of Organismic and Evolutionary Biology, Harvard University, Cambridge, MA 02138, USA
[2]Isotope Bioscience Laboratory – ISOFYS, Faculty of Bioscience Engineering, Ghent University, Ghent, Belgium
[3]Department of Earth and Environment, Boston University, Boston, MA 02215, USA
[4]Département de géographie, Université de Montréal, Montréal, QC, Canada
[5]Lafayette College, Easton, PA 18042, USA
[6]Lincoln University, Jefferson City, MO 65101, USA
[7]The University of North Carolina at Chapel Hill, Chapel Hill, NC 27514, USA

Received: 10 January 2014 – Accepted: 17 January 2014 – Published: 11 February 2014

Correspondence to: S. T. Klosterman (klosterman@fas.harvard.edu)

Published by Copernicus Publications on behalf of the European Geosciences Union.

Abstract

Plant phenology regulates ecosystem services at local and global scales and is a sensitive indicator of global change. Estimates of phenophase transition dates, such as the start of spring or end of autumn, can be derived from sensor-based time series data at the near-surface and remote scales, but must be interpreted in terms of biologically relevant events. We use the PhenoCam archive of digital repeat photography to implement a consistent protocol for visual assessment of canopy phenology at 13 temperate deciduous forest sites throughout eastern North America, as well as to perform digital image analysis for time series-based estimates of phenology dates. We then compare these near-surface results to remote sensing metrics of phenology at the landscape scale, derived from the Moderate Resolution Imaging Spectroradiometer (MODIS) and Advanced Very High Resolution Radiometer (AVHRR) sensors. We present a new type of curve fit, using a generalized sigmoid, to estimate phenology dates. We quantify the statistical uncertainty of phenophase transition dates estimated using this method and show that the generalized sigmoid results in less statistical uncertainty than other curve-fitting methods. Additionally, we find that dates derived from analysis of high-frequency PhenoCam imagery have smaller uncertainties than remote sensing metrics of phenology, and that dates derived from the remotely-sensed enhanced vegetation index (EVI) have smaller uncertainty than those derived from the normalized difference vegetation index (NDVI). Near-surface time series estimates for the start of spring are found to closely match visual assessment of leaf out, as well as remote sensing-derived estimates of the start of spring. However late spring and autumn phenology exhibit larger differences between near-surface and remote scales. Differences in late spring phenology between near-surface and remote scales are found to correlate with a landscape metric of deciduous forest cover. These results quantify the effect of landscape heterogeneity when aggregating to the coarser spatial scales of remote sensing, and demonstrate the importance of accurate curve fitting and vegetation index selection when analyzing and interpreting phenology time series.

BGD
11, 2305–2342, 2014

1 Introduction

Plant phenology plays a central role in how climate change interacts with the biosphere and affects ecosystem services, trophic interactions and species ranges (Richardson et al., 2013a; Morisette et al., 2009). Phenological monitoring throughout past decades and centuries therefore provides a valuable record of how plants have responded to a changing world (Aono and Kazui, 2008; Menzel, 2000; Sparks and Carey, 1995). While direct visual assessment of the phenological status of plants has provided long term records of specific phenophases such as budburst and leaf-out, sensors such as radiometers and digital cameras are now being used to create automated, high frequency, phenological time series (Richardson et al., 2013b). Sensor-based data range from the local scale of site based measurements, to the global extent of satellite missions (Garrity et al., 2011; Huemmrich et al., 1999; Jenkins et al., 2007; Soudani et al., 2012). A key challenge in the interpretation of phenology derived from sensor time series is determining how they relate to plant biological events that an observer would recognize. Digital repeat photography of terrestrial ecosystems serves two purposes in this regard, supplying both a visually interpretable record, and, through image processing techniques, time series data similar to that available from radiometers (Richardson et al., 2007; Sonnentag et al., 2012). Digital repeat photography can therefore serve as a bridge between the traditional practice of direct visual observation of organisms, and sensor-based estimates of phenology from near-surface and remote sensing data.

Digital repeat photography also makes consistent visual assessment of phenology possible over a broad geographic range, as a single set of observers can view many sites with relative ease via digital image archives. In previous comparisons of local to landscape scale phenology, investigators were limited by the ground area a group of observers could feasibly cover on foot (Liang et al., 2011). At the continental scale, comparison of ground-based phenology indicators to remote sensing was limited by the geographic extent of any given mode of ground observation (White et al., 2009).

BGD
11, 2305–2342, 2014

Consequently, there is a knowledge gap in how time series data relate to the biological events of canopy phenology, over a wide geographic range of sites.

This study applied quantitative analysis and visual assessment to a collection of digital repeat photography from a range of deciduous forests across eastern North America. The study sites exhibit diverse landscape characteristics, from a nearly pure deciduous broadleaf forest in Arkansas, to an urban stand of trees in Washington, DC. We compared an ensemble of previously presented and new methods for extracting dates from phenological time series, and quantified the statistical uncertainty of estimated dates. Building on an earlier comparison study by Hufkens et al. (2012), we also analyzed time series data from the Moderate Resolution Imaging Spectroradiometer (MODIS), as well as the MODIS and Making Earth System Data Records for Use in Research Environments (MEASURES) phenology products, for comparison to near-surface estimates. This study aims to evaluate how visually assessed biological events correspond to time series estimates of phenological dates. A complementary goal is to explore how near-surface metrics of deciduous canopy phenology in the spring and fall are related to landscape scale metrics of remote sensing across diverse forest ecosystems.

2 Methods

2.1 Study sites

To characterize leaf phenology of temperate deciduous forests over a broad geographic distribution, we chose 13 sites in the eastern US and Canada, based on availability of near-surface camera observations (Fig. 1). According to the International Geosphere-Biosphere Programme land cover classification scheme of the MODIS Land Cover product (Friedl et al., 2002), at 500 m spatial resolution, six of the sites were dominated by the deciduous broad leaf land cover type, six were dominated by mixed deciduous-coniferous forest, and one site was urban. Finer resolution land cover analysis was

BGD
11, 2305–2342, 2014

carried out using 30 m National Land Cover Database (NLCD) data for sites in the US, to more accurately characterize heterogeneity in land cover type, as reported in Table 1 (Vogelmann et al., 2001). A total of 77 site-years of collocated near-surface and remote sensing imagery were analyzed across all sites.

2.2 Near-surface imagery: visual assessment of phenological transitions

Near-surface imagery was obtained from the PhenoCam archive of digital repeat photography for phenological observation (http://phenocam.sr.unh.edu) and used to visually identify deciduous canopy transition dates. Six observers looked through daily images and used a common protocol to identify these dates for all site-years of data:

1. when the majority of trees started leafing out;
2. when the canopy reached full maturity;
3. when the canopy first started to change color in the fall;
4. when the canopy exhibited the brightest fall colors;
5. when the majority of trees had lost all leaves.

To reduce inter-observer variability in visually assessed dates, the minimum and maximum estimates of each date were discarded, and the remaining dates were averaged to provide a single date for each event. Using the median observation (not reported here) gave similar results to the mean.

2.3 Near-surface imagery: time series estimates of phenological transitions

To automatically extract phenology transition dates from near-surface images, we defined regions of interest (ROIs) representing the deciduous canopy in the foreground at each site as shown in Fig. 2, and analyzed them using software written in Matlab (R2013a, The Mathworks, Nattick, MA), available at https://github.com/klostest/

BGD
11, 2305–2342, 2014

PhenoCamAnalysis. To quantify phenological status of the forest canopy over time, we calculated green chromatic coordinate (GCC) for each image from average red (R), green (G), and blue (B) pixel digital numbers (DNs) over the ROI according to Eq. (1)

$$\mathrm{GCC} = \frac{G}{R+G+B} \tag{1}$$

GCC time series were filtered by discarding images where low average values of R, G, or B DNs in the ROI indicated imagery was too dark to extract phenological data, using site-dependent thresholds. Final processing consisted of selecting the 90th percentile value from a three day moving window (Sonnentag et al., 2012). To quantify dynamics in canopy redness in autumn, red chromatic coordinate (RCC) was calculated in the same way:

$$\mathrm{RCC} = \frac{R}{R+G+B} \tag{2}$$

2.4 Remote sensing data

We downloaded remote sensing data for the 13 study sites through the MODIS web service (http://daac.ornl.gov/MODIS/MODIS-menu/modis_webservice.html) for comparison to near-surface observations. Nadir bidirectional reflectance distribution function (BRDF) adjusted surface reflectances (NBAR) from the MCD43A4 product in the R, near infrared (NIR), and B bands were used to characterize vegetation greenness at 500 m spatial resolution (Schaaf et al., 2002, 2011). Each NBAR measurement is based on surface reflectances taken from a 16 day moving window of MODIS data, and is produced every 8 days. NBAR measurements were associated with the middle day of the 16 day compositing period from which the measurements were drawn (Zhousen Wang and Crystal Schaaf, personal communication, 2013). These data were filtered to remove observations over urban areas, ice, or water according to the MODIS MCD12Q1 Land Cover Type product. Remaining data were filtered to remove interference from snow using the MODIS MCD43A2 BRDF albedo quality product. Filtered

BGD
11, 2305–2342, 2014

NBAR reflectances were combined into the enhanced vegetation index (NBAR-EVI), and the normalized difference vegetation index (NBAR-NDVI) metrics of canopy greenness (Huete et al., 2002; Rouse et al., 1973):

$$\text{NBAR-EVI} = \frac{2.5(\text{NIR} - R)}{(\text{NIR} + 6R - 7.5B + 1)} \quad (3)$$

$$\text{NBAR-NDVI} = \frac{(\text{NIR} - R)}{(\text{NIR} + R)} \quad (4)$$

Median values of NBAR indices were taken over 3×3 spatial windows of 500 m pixels centered on PhenoCam locations, to account for inherent noise in MODIS data due to cloud cover, atmospheric interference, and uncertainty in the ground area measured by the MODIS sensor (Xin et al., 2013). Remote sensing data were then smoothed using the median of a 3 point moving window to remove spikes due to snowfall that were not captured using the MCD43A2 product.

In addition to these remote sensing time series data, we utilized two existing remote sensing phenology products. The MODIS Land Cover Dynamics Product (MCD12Q2) provides annual phenophase transition dates and related growing season metrics at 500 m spatial resolution. The MCD12Q2 algorithm fits logistic functions of the form shown in Eq. (5) to smoothed and gap-filled time series of NBAR-EVI data, and reports local maxima and minima in the rate of change of curvature as phenophase transition dates for the start and end of spring and fall (Ganguly et al., 2010; Zhang et al., 2003). Recently, this algorithm was applied to a 30 yr archive of multi-sensor harmonized vegetation indices created as part of the National Aeronautics and Space Administration (NASA) MEASURES program (http://vip.arizona.edu). The MEASURES phenology product reports similar metrics to the MCD12Q2 algorithm, but has the advantage of nearly twenty additional years of historical data, with measurements from the Advanced Very High Resolution Radiometer (AVHRR). MEASURES phenology data is produced at a spatial resolution of 0.05°, or approximately 5 km for the region studied here.

BGD
11, 2305–2342, 2014

2.5 Estimating dates from time series data

We used three sigmoid-based methods and a data smoothing and interpolation method to examine a diversity of approaches for extracting dates from phenological time series data. The simplest sigmoid-based method, here called the simple sigmoid, has been widely used in the remote sensing community (Hufkens et al., 2012; Liang et al., 2011; Zhang et al., 2003):

$$f(t) = \frac{c}{1 + \exp(a + bt)} + d \tag{5}$$

In Eq. (5), $f(t)$ represents the value of a vegetation index, such as GCC, at time t. d defines the dormant season baseline value of greenness, c is the amplitude of increase in greenness, a controls the timing of increase, and b controls the rate of increase. The same model was used in an analogous manner for the decrease of greenness in autumn. This model was separately fit to spring and fall data for each site year to account for independent green-up and green-down dynamics, using the Matlab function lsqnonlin.

Elmore et al. (2012) presented a modified double sigmoid model to account for the phenomenon of decreasing summer time greenness with parameter m_7, providing more accurate model representation of seasonal vegetation time series data:

$$f(t) = m_1 + (m_2 - m_7 t)\left[\frac{1}{1 + \exp((m_3 - t)/m_4)} - \frac{1}{1 + \exp((m_5 - t)/m_6)}\right] \tag{6}$$

For this study, the green-down sigmoid model in Eq. (6) was fit to whole years of vegetation index time series.

These two previously presented sigmoid models were compared with a more flexible approach, using a generalized sigmoid formula which allows for different rates of increase near the lower and upper asymptotes of the sigmoid, with parameters q_i and v_i (Richards, 1959). Our implementation of the generalized sigmoid also accounts for

BGD
11, 2305–2342, 2014

non-linear decrease in summer time greenness, as observed in many site-years of data, with parameters a_2 and b_2, as well as a changing dormant season value with parameter a_1:

$$f(t) = (a_1 t + b_1) + (a_2 t^2 + b_2 t + c)\left[\frac{1}{[1 + q_1 \exp(-b_1(t - m_1))]^{v_1}} - \frac{1}{[1 + q_2 \exp(-b_2(t - m_2))]^{v_2}}\right] \quad (7)$$

Equation (7), here called the generalized sigmoid, was fit to entire years of data.

For the sigmoid models, phenological transition dates were estimated using local extrema in the rate of change of curvature k (Kline, 1998):

$$k = \frac{f''(t)}{(1 + (f'(t))^2)^{\frac{3}{2}}} \quad (8)$$

Points where the curvature changes most rapidly, also referred to as inflection points, occur at the beginning, middle, and end of seasonal transitions. In the simple and greendown sigmoids, extrema in the curvature change rate were used to identify the start, middle, and end of spring (SOS, MOS, and EOS), following the method proposed by Zhang et al. (2003). These points approximately correspond to 10 %, 50 %, and 90 % of amplitude in springtime greenness. A similar technique was used for the start, middle, and end of fall (SOF, MOF, and EOF). For the generalized sigmoid, the third extrema in the curvature change rate was used to identify the end of spring, however the first two extrema were found to occur significantly later than 10 % and 50 % of amplitude in springtime greenness. Consequently the start and middle of spring were identified as the times of 10 % and 50 % amplitude between the dormant season and the end of spring values of greenness for the generalized sigmoid, with a similar approach used in fall.

To quantify uncertainty of date estimates from the sigmoid-based methods, we used the Jacobian matrix of parameter sensitivities, output from the Matlab routine lsqnonlin,

BGD
11, 2305–2342, 2014

to calculate the parameter covariance matrix. The covariance matrix was then used in a Monte Carlo procedure to generate 100 samples of parameter space, each of which was used to produce a new set of phenology dates. Monte Carlo ensembles were used to construct confidence intervals using the inner 95 % range for each phenology date, referred to here as statistical uncertainty of estimated dates.

In the smoothing and interpolation approach, time series data were first smoothed using the loess algorithm in Matlab, which reduces noise by estimating a local regression to a second order polynomial at each point in the time series. The fraction of annual data used for the local regression was set to 0.1 for near-surface data and 0.2 for remote sensing data, to account for the different temporal resolutions of 3 and 8 days, respectively. After smoothing, cubic spline interpolation was applied to obtain a fine-grained time series for estimating phenological transitions. Spring transition dates were identified as the times when greenness crossed 10 %, 50 %, and 90 % thresholds of the springtime amplitude in greenness. The smoothing and interpolation method was also applied to RCC time series in autumn, where a single phenology date was identified as the fall maximum of the processed time series. To illustrate each of the date estimation methods, an example year of data from Arbutus Lake in 2009 is shown in both near-surface and remote sensing data (Fig. 3), with model fits and date estimates for each approach.

To compare visual assessment, near-surface, and remotely sensed phenology dates, the root mean square deviation (RMSD), bias, and r^2 statistic were computed for each phenological transition across all site-years of data. These statistics indicate the magnitude of the difference between corresponding dates from various methods, the average signed difference, and the degree of correlation, respectively.

BGD
11, 2305–2342, 2014

3 Results

3.1 Statistical uncertainty in date estimates

We used inter-observer variability from visual assessment and parameter uncertainty of curve fitting methods to calculate measures of the statistical uncertainty of phenology date estimates from near-surface digital photography. The average range of date estimates from visual assessment was larger than the average inner 95 % confidence interval from curve fitting of GCC data for both spring phenology dates, particularly at the end of spring (Table 2). However in autumn, inter-observer variability was smaller than the statistical uncertainty of curve fitting for the middle and end of fall. These results indicate that curve fitting analysis of greenness time series is generally more precise than visual assessment in the spring, but less so in the fall.

In the analysis of statistical uncertainty from different spatial scales of time series data, near-surface GCC data supported more certainty in estimates of phenology dates (average 6 day confidence interval, across methods and dates reported in Table 2) than NBAR-EVI and NBAR-NDVI data of remote sensing (average 12 and 19 day confidence intervals, respectively). This may be due to the higher temporal resolution of near-surface data, which more effectively constrains parameter estimates. Since NBAR-EVI data was found to result in less uncertainty for remote sensing estimates of phenology than NBAR-NDVI, these results are emphasized in the following analysis.

Of the sigmoid methods, the generalized sigmoid curve fit the time series data with the lowest RMSD and produced the least uncertain date estimates in most cases, particularly with the near-surface data (Table 2). From NBAR-EVI data, the simple sigmoid function identified the middle of spring transition with the lowest uncertainty. However the greendown sigmoid and the generalized sigmoid curves resulted in more certain date estimates at the beginning and end of spring, respectively. The generalized sigmoid appears to be the most balanced functional representation of vegetation dynamics for NBAR-EVI in terms of certainty from the beginning to end of spring, likely because of its flexibility. Therefore results presented here will consider the ensemble of

BGD
11, 2305–2342, 2014

time series approaches including all sigmoid types, as well as smoothing and interpolation, with emphasis on the generalized sigmoid.

3.2 Comparison of visual assessment to estimates from near-surface time series data

Visual assessment exhibited varying degrees of correspondence to dates identified using time series data, depending on the date estimation method and seasonal transition (Table 3). The start of spring was most closely associated with visual assessment of the date when the majority of trees started to leaf out (Fig. 4a). For this date, all time series methods matched visual assessment with an RMSD of less than 10 days, the generalized sigmoid yielding the lowest bias of 0 days. The visually assessed date of canopy maturity had a less consistent relation to time series estimates than the date of leaf out. While correlation was generally good, with r^2 ranging from 0.45 to 0.73 across methods, all time series estimates for this date were biased about 10 days earlier than visual assessment. For the generalized sigmoid method, the end of spring was less biased with respect to visual assessment for spring transitions that ended later in the year (Fig. 4b).

Greenness-derived estimates for the beginning and end of autumn generally showed less agreement with visual assessment than for spring phenology; autumn estimates derived from greenness time series had larger average RMSD (23 and 16 days, respectively, from Table 3) across methods than either of the spring dates (8 days for the start of spring and 13 days for the end of spring). Autumn dates derived using the generalized sigmoid had equal or lower RMSD from visually assessed dates than dates from other curve fitting approaches, and indicated that the estimate for end of autumn was generally less biased with respect to visual assessment of abscission when this transition occurred later in the calendar year (Fig. 4e). While the visually assessed start of color change in autumn and the end of abscission were closer to greenness derived metrics, timing of the brightest fall colors had similar RMSD with respect to date estimates from time series of both redness and greenness (Table 3).

BGD
11, 2305–2342, 2014

3.3 Comparison of near-surface and remote sensing phenology

The generalized sigmoid model, the time series method with the least uncertainty, and the smoothing and interpolation approach, with the most flexibility, each produced an average RMSD of about 9 days between remote sensing and near-surface imagery across the beginning, middle, and end of spring dates (Table 4, Fig. 5a–c). The magnitude (absolute value) of bias was low across all methods for the beginning and middle of spring, less than one week in nearly all cases (Table 4). As spring progressed however, the signed bias between remote sensing and near-surface phenology became more negative, indicating remote sensing was later in comparison to near-surface. The trend of a more negative bias for later spring phenology dates was not isolated to one particular method; across all methods and indices, remote sensing was an average of 2 and 8 days later than near-surface metrics for the middle and end of spring, respectively (Table 4).

To examine whether landscape characteristics of individual sites played a role in the late spring bias, we calculated the fractional coverage of deciduous forest and mixed forest land cover types from NLCD data (Table 1). The bias between near-surface GCC and remote sensing NBAR-EVI with the generalized sigmoid method (Fig. 6) showed a significant trend ($r^2 = 0.87$, $p < 0.001$) toward less bias for sites that had a greater fraction of deciduous or mixed forest coverage.

Time series estimates of autumn phenology from near-surface and remote scales generally differed more than spring dates; the average RMSD for autumn dates was higher than spring in all methods and indices used for date estimation (Table 4). This is likely due to larger statistical uncertainty in estimated autumn dates; GCC, NBAR-EVI and NBAR-NDVI derived dates were roughly twice as uncertain as those in spring (Table 2). GCC derived near-surface autumn dates from the generalized sigmoid method were biased roughly a week earlier than remote sensing dates, emblematic of a negative bias for autumn dates observed across most greenness time series results, particularly for the middle and end of fall. In contrast, near-surface dates derived from

BGD
11, 2305–2342, 2014

redness, which best corresponded to the middle of fall date extracted from remote sensing (Table 5), were consistently positively biased. Both greenness and redness derived near-surface dates had the lowest magnitude of bias at the MOF date, with several methods producing a bias of less than a week.

3.4 Comparison of near-surface phenology to MCD12Q2 and MEASURES phenology products

The MCD12Q2 and MEASURES phenology products gave remotely sensed phenology estimates at different spatial scales than the analysis of NBAR data presented above. The MCD12Q2 phenology product is produced at 500 m resolution, the NBAR analysis conducted for this study used MODIS data at an effective resolution of 1.5 km due to spatial windowing, and MEASURES is produced at approximately 5 km resolution. In comparison to NBAR data analyzed here, the phenology products exhibited similar signs in bias, but different magnitudes, with respect to date estimates from near-surface time series. The coarse resolution MEASURES spring dates exhibited a low average bias of less than two days at the beginning of spring, while middle of spring and end of spring were progressively biased later by an average of −9 and −17 days, respectively (Table 6), similar to the late spring bias presented above, but larger in magnitude. RMSD's between MEASURES and near-surface dates were also larger than NBAR data, by over a week for most transition dates. The MCD12Q2 product, encompassing the smallest land area of the three remote sensing analyses used here, showed qualitatively similar characteristics to the coarse scale MEASURES results, but with larger average RMSD (Table 7). In consideration of the analysis presented above, results from MEASURES and MCD12Q2 indicate that remote sensing data from an intermediate spatial scale between these two products, processed with the methods presented here, may result in better agreement with near-surface data.

BGD
11, 2305–2342, 2014

4 Discussion

The amount of phenological data available from near-surface and remote sensing measurements presents a large and growing resource for monitoring the interaction between global change and the biosphere, but also a challenge for analysis. For example, lack of standard protocols complicates determination of which biological events correspond to data-driven estimates of phenophase transitions in diverse and geographically dispersed ecosystems (White et al., 2009). Furthermore, while several methods exist for estimation of transition dates from time series data, few studies indicate how to distinguish between these approaches (but see Cong et al., 2012), or quantify the uncertainty associated with various methods. This study compared an ensemble of date estimation methods to assess how near-surface metrics of deciduous forest phenology, here derived from high-frequency digital camera imagery, relate to both visual assessment of canopy status, and to landscape scale estimates from remote sensing platforms, across a range of temperate deciduous forests. Our results show that the choice of analysis method affects the certainty with which dates can be estimated at both near-surface and remote scales. The choice of analysis method can also affect the RMSD, magnitude of bias, and in some cases the direction of bias in the comparison of near-surface phenology metrics to visual assessment and remote sensing.

4.1 Comparison of near-surface estimates to visual assessment and remote sensing in spring

Time series estimates of the start of spring at the near-surface scale are generally well-correlated with visual assessment of the first appearance of leaves (Fig. 4a), although a significant outlier resulted from the spring of 2007 at the Upper Buffalo Wilderness. Observers consistently identified the start of leaf-out as DOY 90, earlier than other years for this site. However after this early leaf-out, a spring frost delayed further leaf development (Gu et al., 2008), likely resulting in the later start of spring (DOY 120) identified by curve fitting analysis.

BGD
11, 2305–2342, 2014

Start of spring was also highly correlated between remote sensing and near-surface, in agreement with previous studies. Liang et al. (2011) noted that start of spring estimated from MODIS EVI time series matched the date of budburst directly observed on trees to within two days in a mixed deciduous coniferous forest in Wisconsin, and Soudani et al. (2008) found a similar result for deciduous forests located throughout France. A recent study by Hmimina et al. (2013) also found good agreement between near-surface and remote sensing of the beginning of spring. However we found that data-driven estimates of later spring phenology from near-surface imagery, intended to represent the final stages of springtime leaf development, exhibited less correspondence to both visual assessment and remote sensing.

The visually assessed date of leaf maturity was later than the end of spring date derived from near-surface GCC. Recent research suggests explanations for this: at Harvard Forest, leaves were found to have higher GCC values during expansion than at the later stages of maturity marked by greater leaf mass per area (LMA), and higher leaf area index (LAI) (Keenan et al., 2014). Accordingly, the earlier springtime peak in GCC than in LMA and LAI may influence the bias between estimated and visually assessed dates seen here, as well as the oblique viewing angle of PhenoCams explored by Keenan et al. The bias is more pronounced for earlier ends of spring (Fig. 4), suggesting that in later ends of spring, leaves may mature to higher LMA and canopies to greater LAI more quickly after expanding.

In the comparison between near-surface and remote sensing of late spring phenology, results show that across all date estimation approaches, remote sensing was biased later by an average of 8 days (Table 4). Hmimina et al. (2013) found a similar late spring bias using NDVI from remote sensing and near-surface NDVI sensors, indicating the bias is not likely due to differences in vegetation indices used at the near-surface and remote scales, such as the GCC and NBAR-EVI used here. The site-based analysis of late spring bias (Fig. 6) suggests a relationship between landscape composition and the length of the late spring bias. In sites with a smaller fraction of deciduous and mixed forests, and a greater proportion of woody wetlands, evergreens,

BGD
11, 2305–2342, 2014

and other land cover types, remotely sensed end of spring was progressively later than near-surface estimates. Researchers have explored the effect of vegetation heterogeneity on the comparison of near-surface, point measurements and remotely sensed, pixel measurements of albedo across multiple sites (Cescatti et al., 2012), finding that more homogeneous sites produced better agreement between scales. However this study appears to be the first to document a linear correlation between forest coverage and temporal bias in canopy phenology between the organism and pixel scales, indicating how landscape characteristics may determine the fidelity of remote sensing to near-surface measurements.

4.2 Comparison of near-surface estimates to visual assessment and remote sensing in fall

In fall, variability between observers was smaller for the dates of brightest fall colors and leaf abscission than for the first signs of senescence (Table 2), indicating that the brilliant fall colors associated with the middle of senescence, and the eventual loss of leaves, give the clearest visual indicators of autumn phenology. Data-driven estimates using peak redness from near-surface images matched the visual assessment of brightest fall colors with similar RMSD to greenness-based estimates of the middle of fall (Table 3), with peak redness biased 3 days later and greenness biased 2–6 days earlier.

We found that the statistical uncertainty in curve fit estimates of autumn dates was larger than that of spring dates (Table 2). This may be due to within-canopy heterogeneity, with some trees senescing before others, exemplified in Fig. 2 where certain trees are in advanced stages of senescence while others still have many green leaves. Integrating all of these trees into a single region of interest tends to cause a longer, more drawn out transition in autumn than in spring (Fig. 3). This more gradual change leads to less well-defined extrema in the curvature change rate (Eq. 8) of GCC time series, and consequently greater statistical uncertainty in estimated autumn dates than spring dates. Based on this alone, we would expect larger RMSD between camera- and

BGD
11, 2305–2342, 2014

satellite-derived dates in autumn than spring. On a larger scale, variation in species composition and land cover type also complicates the interpretation of NBAR-EVI and NBAR-NDVI measurements in autumn (Cescatti et al., 2012; Dragoni and Rahman, 2012), similar to effects on near-surface GCC and RCC (Richardson et al., 2009).

To more accurately study spatial variation in autumn phenology, and to further study the late spring bias in heterogeneous forested landscapes reported above, photography of larger fields of view, and more plants and plant functional types, should be obtained (Hufkens et al., 2012). Use of multiple cameras at a single site, and multiple regions of interest on a given image (Richardson et al., 2009) would enable more complete characterization of these heterogeneous phenological phenomena.

4.3 Remote sensing phenology products

While the simple sigmoid approach used here with NBAR data is identical to that used for the MCD12Q2 and MEASURES products, these products encompass different land areas, leading to divergent results. MCD12Q2 does not use the spatial windowing approach employed here, but represents the remote sensing measurements associated with a single 500 m pixel. Therefore the MCD12Q2 data are more susceptible to gridding artifacts of remote sensing measurements, which arise from the fact that only roughly 30 % of MODIS observations measure the reported pixel location on the land surface (see Fig. 1 in Xin et al., 2013). A spatial windowing approach, accounting for the values of neighboring pixels, appears to improve the remote sensing representation of deciduous canopy phenology in comparison to near-surface measurements: the simple sigmoid method comparison conducted here deviated from that of the MCD12Q2 product, exhibiting generally lower RMSD and bias with respect to ground measurements (Tables 4 and 7). The larger land area of measurements used to derive the MEASURES phenology product also resulted in greater similarity to near-surface phenology dates than MCD12Q2 (Table 6).

BGD
11, 2305–2342, 2014

5 Conclusions

This study used near-surface digital repeat photography to derive both visual assessment and time series estimates of leaf phenology, over a broad geographic range of temperate deciduous forests. To then evaluate landscape scale phenology metrics from remote sensing with near-surface metrics, a common framework of curve fitting methods was applied to estimate phenophase transition dates at both scales. Results indicate that visual assessment of the start of leaf-out in spring was very similar to estimates of the start of spring from digital image processing, and across the jump in scale from near-surface to remote. However in later spring, study sites with more heterogeneous land cover exhibited greater differences between near-surface and remote sensing phenology. In particular, remote sensing of late spring phenology was biased later than near-surface, with progressively larger bias for ecosystems with a lower fraction of forest cover.

These results have broad implications for the quantification of ecosystem services that depend on accurate monitoring of phenological events. For example, remote sensing data is used to infer the phenology of deciduous trees in ecosystem and earth system models (Lawrence et al., 2011; Medvigy et al., 2009). If an artificially late end of spring is detected in regions with smaller fractions of forest cover, this may lead to later attainment of full photosynthetic capacity in the modeled canopy, resulting in lower estimates of annual sums of net productivity in forest ecosystems (Goulden et al., 1996; Richardson et al., 2012). Near-surface imagery could be used in such ecosystems to separate phenological signals of diverse land cover types, for more accurate quantification of ecosystem services.

In addition to dependence on site heterogeneity, this study found that both the analysis methods and data sources for phenological time series affect the certainty of derived dates and the nature of the comparison of near-surface to remote sensing data. Dates derived from the NBAR-EVI index of remote sensing had less statistical uncertainty than dates calculated using NBAR-NDVI. Analysis methods with more flex-

BGD
11, 2305–2342, 2014

ibility for describing seasonal variation in vegetation greenness, particularly a novel generalized sigmoid method, resulted in higher certainty of estimated dates and better agreement with visual assessment of canopy phenology, demonstrating the importance of accurate functional representation of phenological time series for identification of phenophase transition dates.

Acknowledgements. Isaac Lavine, Lakeitha Mitchell, and Rachel Norman were supported by the Harvard Forest Summer Research Program in Forest Ecology through grants from the National Science Foundation's Research Experiences for Undergraduates program (award DBI-1003938) and NASA's Global Climate Change Education program. The Richardson Lab acknowledges support from the Northeastern States Research Cooperative, NSF's Macrosystems Biology program (award EF-1065029), the US National Park Service Inventory and Monitoring Program and the USA National Phenology Network (grant number G10AP00129 from the United States Geological Survey). We thank the USDA Forest Service Air Resource Management program and the National Park Service Air Resources program for contributing camera imagery to this analysis. Research at Harvard Forest is partially supported by the National Science Foundation's LTER program (awards DEB-0 080 592, DEB-1237491). The Friedl Lab at Boston University acknowledges support from NASA grant number NNX11AE75G and the NASA MEASURES program via subcontract number Y502545 from the University of Arizona. The contents of this paper are solely the responsibility of the authors and do not necessarily represent the official views of NSF, USGS, or NASA.

References

Aono, Y. and Kazui, K.: Phenological data series of cherry tree flowering in Kyoto, Japan, and its application to reconstruction of springtime temperatures since the 9th century, Int. J. Climatol., 28, 905–914, doi:10.1002/joc.1594, 2008.

Cescatti, A., Marcolla, B., Santhana Vannan, S. K., Pan, J. Y., Román, M. O., Yang, X., Ciais, P., Cook, R. B., Law, B. E., Matteucci, G., Migliavacca, M., Moors, E., Richardson, A. D., Seufert, G., and Schaaf, C. B.: Intercomparison of MODIS albedo retrievals and in situ measurements across the global FLUXNET network, Remote Sens. Environ., 121, 323–334, doi:10.1016/j.rse.2012.02.019, 2012.

BGD
11, 2305–2342, 2014

Cong, N., Piao, S., Chen, A., Wang, X., Lin, X., Chen, S., Han, S., Zhou, G., and Zhang, X.: Spring vegetation green-up date in China inferred from SPOT NDVI data: a multiple model analysis, Agr. Forest Meteorol., 165, 104–113, doi:10.1016/j.agrformet.2012.06.009, 2012.

Dragoni, D. and Rahman, A. F.: Trends in fall phenology across the deciduous forests of the Eastern USA, Agr. Forest Meteorol., 157, 96–105, doi:10.1016/j.agrformet.2012.01.019, 2012.

Elmore, A. J., Guinn, S. M., Minsley, B. J., and Richardson, A. D.: Landscape controls on the timing of spring, autumn, and growing season length in mid-Atlantic forests, Glob. Change Biol., 18, 656–674, doi:10.1111/j.1365-2486.2011.02521.x, 2012.

Friedl, M., McIver, D., Hodges, J. C., Zhang, X., Muchoney, D., Strahler, A., Woodcock, C., Gopal, S., Schneider, A., Cooper, A., Baccini, A., Gao, F., and Schaaf, C.: Global land cover mapping from MODIS: algorithms and early results, Remote Sens. Environ., 83, 287–302, doi:10.1016/S0034-4257(02)00078-0, 2002.

Ganguly, S., Friedl, M. A., Tan, B., Zhang, X., and Verma, M.: Land surface phenology from MODIS: characterization of the Collection 5 global land cover dynamics product, Remote Sens. Environ., 114, 1805–1816, doi:10.1016/j.rse.2010.04.005, 2010.

Garrity, S. R., Bohrer, G., Maurer, K. D., Mueller, K. L., Vogel, C. S., and Curtis, P. S.: A comparison of multiple phenology data sources for estimating seasonal transitions in deciduous forest carbon exchange, Agr. Forest Meteorol., 151, 1741–1752, doi:10.1016/j.agrformet.2011.07.008, 2011.

Goulden, M. L., Munger, J. W., Fan, S. M., Daube, B. C., and Wofsy, S. C.: Exchange of carbon dioxide by a deciduous forest?: response to interannual climate variability, Science, 271, 1576, doi:10.1126/science.271.5255.1576, 1996.

Gu, L., Hanson, P. J., Post, W. M., Kaiser, D. P., Yang, B., Nemani, R., Pallardy, S. G., and Meyers, T.: The 2007 Eastern US spring freeze: increased cold damage in a warming world, Bioscience, 58, 253, doi:10.1641/B580311, 2008.

Hmimina, G., Dufrêne, E., Pontailler, J.-Y., Delpierre, N., Aubinet, M., Caquet, B., de Grandcourt, A., Burban, B., Flechard, C., Granier, A., Gross, P., Heinesch, B., Longdoz, B., Moureaux, C., Ourcival, J.-M., Rambal, S., Saint André, L., and Soudani, K.: Evaluation of the potential of MODIS satellite data to predict vegetation phenology in different biomes: an investigation using ground-based NDVI measurements, Remote Sens. Environ., 132, 145–158, doi:10.1016/j.rse.2013.01.010, 2013.

BGD
11, 2305–2342, 2014

Huemmrich, K. F., Black, T. A., Jarvis, P. G., McCaughey, J. H., and Hall, F. G.: High temporal resolution NDVI phenology from micrometeorological radiation sensors, J. Geophys. Res., 104, 27935, doi:10.1029/1999JD900164, 1999.
Huete, A., Didan, K., Miura, T., Rodriguez, E., Gao, X., and Ferreira, L.: Overview of the radiometric and biophysical performance of the MODIS vegetation indices, Remote Sens. Environ., 83, 195–213, doi:10.1016/S0034-4257(02)00096-2, 2002.
Hufkens, K., Friedl, M., Sonnentag, O., Braswell, B. H., Milliman, T., and Richardson, A. D.: Linking near-surface and satellite remote sensing measurements of deciduous broadleaf forest phenology, Remote Sens. Environ., 117, 307–321, doi:10.1016/j.rse.2011.10.006, 2012.
Jenkins, J. P., Richardson, A. D., Braswell, B. H., Ollinger, S. V., Hollinger, D. Y., and Smith, M. L.: Refining light-use efficiency calculations for a deciduous forest canopy using simultaneous tower-based carbon flux and radiometric measurements, Agr. Forest Meteorol., 143, 64–79, doi:10.1016/j.agrformet.2006.11.008, 2007.
Keenan, T. F., Darby, B., Felts, E., Sonnentag, O., Friedl, M., Hufkens, K., O'Keefe, J., Klosterman, S., Munger, J. W., Toomey, M., and Richardson, A. D.: Tracking forest phenology and seasonal physiology using digital repeat photography: a critical assessment, Ecol. Appl., in press, 2014.
Kline, M.: Calculus: an Intuitive and Physical Approach, 2nd edn., Dover Books on Mathematics, Dover Publications, 1998.
Lawrence, D. M., Oleson, K. W., Flanner, M. G., Thornton, P. E., Swenson, S. C., Lawrence, P. J., Zeng, X., Yang, Z.-L., Levis, S., Sakaguchi, K., Bonan, G. B., and Slater, A. G.: Parameterization improvements and functional and structural advances in Version 4 of the Community Land Model, J. Adv. Model. Earth Syst., 3, 1–27, doi:10.1029/2011MS000045, 2011.
Liang, L., Schwartz, M. D., and Fei, S.: Validating satellite phenology through intensive ground observation and landscape scaling in a mixed seasonal forest, Remote Sens. Environ., 115, 143–157, doi:10.1016/j.rse.2010.08.013, 2011.
Medvigy, D., Wofsy, S. C., Munger, J. W., Hollinger, D. Y., and Moorcroft, P. R.: Mechanistic scaling of ecosystem function and dynamics in space and time: Ecosystem Demography model version 2, J. Geophys. Res., 114, G01002, doi:10.1029/2008JG000812, 2009.
Menzel, A.: Trends in phenological phases in Europe between 1951 and 1996, Int. J. Biometeorol., 44, 76–81, doi:10.1007/s004840000054, 2000.

BGD
11, 2305–2342, 2014

Morisette, J. T., Richardson, A. D., Knapp, A. K., Fisher, J. I., Graham, E. A., Abatzoglou, J., Wilson, B. E., Breshears, D. D., Henebry, G. M., Hanes, J. M., and Liang, L.: Tracking the rhythm of the seasons in the face of global change: phenological research in the 21st century, Front. Ecol. Environ., 7, 253–260, doi:10.1890/070217, 2009.

Richards, F. J.: A flexible growth function for empirical use, J. Exp. Bot., 10, 290–301, doi:10.1093/jxb/10.2.290, 1959.

Richardson, A. D., Anderson, R. S., Arain, M. A., Barr, A. G., Bohrer, G., Chen, G., Chen, J. M., Ciais, P., Davis, K. J., Desai, A. R., Dietze, M. C., Dragoni, D., Garrity, S. R., Gough, C. M., Grant, R., Hollinger, D. Y., Margolis, H. A., McCaughey, H., Migliavacca, M., Monson, R. K., Munger, J. W., Poulter, B., Raczka, B. M., Ricciuto, D. M., Sahoo, A. K., Schaefer, K., Tian, H., Vargas, R., Verbeeck, H., Xiao, J., and Xue, Y.: Terrestrial biosphere models need better representation of vegetation phenology: results from the North American Carbon Program Site Synthesis, Glob. Change Biol., 18, 566–584, doi:10.1111/j.1365-2486.2011.02562.x, 2012.

Richardson, A. D., Jenkins, J. P., Braswell, B. H., Hollinger, D. Y., Ollinger, S. V., and Smith, M.-L.: Use of digital webcam images to track spring green-up in a deciduous broadleaf forest, Oecologia, 152, 323–334, doi:10.1007/s00442-006-0657-z, 2007.

Richardson, A. D., Braswell, B. H., Hollinger, D. Y., Jenkins, J. P., and Ollinger, S. V.: Near-surface remote sensing of spatial and temporal variation in canopy phenology, Ecol. Appl., 19, 1417–28, 2009.

Richardson, A. D., Keenan, T. F., Migliavacca, M., Ryu, Y., Sonnentag, O., and Toomey, M.: Climate change, phenology, and phenological control of vegetation feedbacks to the climate system, Agr. Forest Meteorol., 169, 156–173, doi:10.1016/j.agrformet.2012.09.012, 2013a.

Richardson, A. D., Klosterman, S., and Toomey, M.: Near-surface sensor derived phenology, in: Phenology: an Integrative Environmental Science, edited by: Schwartz, M. D., Kluwer Academic Publishers, 2013b.

Rouse, J., Haas, R., Schell, J., and Deering, D.: Monitoring vegetation systems in the great plains with ERTS, in: Third ERTS Symposium, vol. 1, NASA SP-351, 309–317, 1973.

Schaaf, C. B., Gao, F., Strahler, A. H., Lucht, W., Li, X., Tsang, T., Strugnell, N. C., Zhang, X., Jin, Y., Muller, J.-P., Lewis, P., Barnsley, M., Hobson, P., Disney, M., Roberts, G., Dunderdale, M., Doll, C., d'Entremont, R. P., Hu, B., Liang, S., Privette, J. L., and Roy, D.: First operational BRDF, albedo nadir reflectance products from MODIS, Remote Sens. Environ., 83, 135–148, doi:10.1016/S0034-4257(02)00091-3, 2002.

BGD
11, 2305–2342, 2014

Schaaf, C. B., Liu, J., Gao, F., and Strahler, A. H.: Aqua and terra MODIS albedo and reflectance anisotropy products, in: Land Remote Sensing and Global Environmental Change, vol. 11, edited by: Ramachandran, B., Justice, C. O., and Abrams, M. J., Springer, New York, 549–561, 2011.

Sonnentag, O., Hufkens, K., Teshera-Sterne, C., Young, A. M., Friedl, M., Braswell, B. H., Milliman, T., O'Keefe, J., and Richardson, A. D.: Digital repeat photography for phenological research in forest ecosystems, Agr. Forest Meteorol., 152, 159–177, doi:10.1016/j.agrformet.2011.09.009, 2012.

Soudani, K., le Maire, G., Dufrêne, E., François, C., Delpierre, N., Ulrich, E., and Cecchini, S.: Evaluation of the onset of green-up in temperate deciduous broadleaf forests derived from Moderate Resolution Imaging Spectroradiometer (MODIS) data, Remote Sens. Environ., 112, 2643–2655, doi:10.1016/j.rse.2007.12.004, 2008.

Soudani, K., Hmimina, G., Delpierre, N., Pontailler, J.-Y., Aubinet, M., Bonal, D., Caquet, B., de Grandcourt, A., Burban, B., Flechard, C., Guyon, D., Granier, A., Gross, P., Heinesh, B., Longdoz, B., Loustau, D., Moureaux, C., Ourcival, J.-M., Rambal, S., Saint André, L., and Dufrêne, E.: Ground-based Network of NDVI measurements for tracking temporal dynamics of canopy structure and vegetation phenology in different biomes, Remote Sens. Environ., 123, 234–245, doi:10.1016/j.rse.2012.03.012, 2012.

Sparks, T. H. and Carey, P. D.: The responses of species to climate over two centuries: an analysis of the Marsham phenological record, 1736–1947, J. Ecol., 83, 13-0652R, 1995.

Vogelmann, J. E., Howard, S. M., Yang, L., Larson, C. R., Wylie, B. K., and Van Driel, N.: Completion of the 1990s National Land Cover Data Set for the conterminous United States from Landsat Thematic Mapper data and ancillary data sources, Photogramm. Eng. Rem. S., 67, 650-662, 2001.

White, M. A., de Beurs, K. M., Didan, K., Inouye, D. W., Richardson, A. D., Jensen, O. P., O'Keefe, J., Zhang, G., Nemani, R. R., van Leeuwen, W. J. D., Brown, J. F., de Wit, A., Schaepman, M., Lin, X., Dettinger, M., Bailey, A. S., Kimball, J., Schwartz, M. D., Baldocchi, D. D., Lee, J. T., and Lauenroth, W. K.: Intercomparison, interpretation, and assessment of spring phenology in North America estimated from remote sensing for 1982–2006, Glob. Change Biol., 15, 2335–2359, doi:10.1111/j.1365-2486.2009.01910.x, 2009.

Xin, Q., Olofsson, P., Zhu, Z., Tan, B., and Woodcock, C. E.: Toward near real-time monitoring of forest disturbance by fusion of MODIS and Landsat data, Remote Sens. Environ., 135, 234–247, doi:10.1016/j.rse.2013.04.002, 2013.

BGD
11, 2305–2342, 2014

Zhang, X., Friedl, M. A., Schaaf, C. B., Strahler, A. H., Hodges, J. C. F., Gao, F., Reed, B. C., and Huete, A.: Monitoring vegetation phenology using MODIS, Remote Sens. Environ., 84, 471–475, doi:10.1016/S0034-4257(02)00135-9, 2003.

BGD
11, 2305–2342, 2014

Table 1. Study sites with land cover characterization. Fractional land coverage of each land cover type was calculated from the NLCD (National Land Cover Database) for study sites located in the US. "Other" includes shrub/scrub, developed; low intensity, developed; medium intensity, grassland/herbaceous, developed; high intensity, emergent herbaceous wetlands, pasture/hay, and barren land (rock/sand/clay).

Site	Deciduous forest	Mixed forest	Evergreen forest	Woody wetlands	Developed; open space	Open water	Other
Acadia	0.11	0.32	0.21	0.02	0.06	0.12	0.17
Arbutus Lake	0.41	0.07	0.13	0.12	0.01	0.23	0.01
Bartlett	0.37	0.48	0.08	0.00	0.05	0.00	0.02
Boundary Waters	0.10	0.24	0.21	0.22	0.04	0.04	0.14
Dolly Sods	0.56	0.04	0.21	0.11	0.06	0.00	0.03
Harvard Forest	0.41	0.22	0.20	0.12	0.04	0.00	0.00
Mammoth Cave	0.67	0.01	0.23	0.05	0.00	0.02	0.02
Washington DC	0.01	0.00	0.00	0.05	0.25	0.24	0.43
Smoky Look	0.72	0.05	0.08	0.00	0.09	0.00	0.06
U. of Michigan Biological Station	0.68	0.06	0.03	0.04	0.05	0.01	0.13
Upper Buffalo	0.97	0.00	0.00	0.00	0.03	0.00	0.00

BGD
11, 2305–2342, 2014

Table 2. Statistical uncertainty in estimated phenology dates. Statistical uncertainty in sigmoid-based methods is calculated as the average width of inner 95 % confidence intervals for each phenology date. SOS, MOS, and EOS are start, middle, and end of spring. SOF, MOF, and EOF are start, middle and end of fall. Statistical uncertainty in visual assessment is calculated as the average length of time between earliest and latest assessments, after removing the minimum and maximum estimates from the raw data. All units are in days.

Index	Time series method	SOS	MOS	EOS	SOF	MOF	EOF
GCC	simple sigmoid	7	3	7	13	7	16
	greendown sigmoid	4	2	6	14	7	11
	generalized sigmoid	1	1	0	3	5	7
EVI	simple sigmoid	9	4	9	24	13	28
	greendown sigmoid	8	5	15	24	14	18
	generalized sigmoid	8	6	8	8	9	12
NDVI	simple sigmoid	16	8	16	24	15	27
	greendown sigmoid	16	11	38	42	30	37
	generalized sigmoid	10	6	10	11	14	18
Visual assessment		7		22	19	4	6

BGD
11, 2305–2342, 2014

Table 3. Statistics comparing visual assessment to phenology derived from near-surface image processing. Visually assessed dates were compared to time series methods as follows: the date when the majority of trees started leafing out was compared to SOS, the date of canopy maturity to EOS, the date of first color change to SOF, the date of brightest fall colors to MOF, and the date of leaf loss to EOF. Near surface imagery dates were estimated from greenness, except for SOF, MOF, and EOF dates in the smoothing and interpolation approach, which were estimated from redness. Statistics include RMSD and bias in units of days, and r^2 for the comparison of corresponding dates and methods across all site-years. Bias is calculated relative to time series estimates, so a negative bias indicates that the corresponding visual assessment is later.

Time series method	Statistic	SOS	EOS	SOF	MOF	EOF
simple sigmoid	RMSD	8	16	17	9	16
	Bias	3	−14	5	−6	−11
	r^2	0.79	0.69	0.45	0.80	0.64
greendown sigmoid	RMSD	7	13	22	9	16
	Bias	3	−11	16	−2	−14
	r^2	0.81	0.73	0.60	0.77	0.70
generalized sigmoid	RMSD	7	11	16	9	12
	Bias	0	−9	3	−6	−8
	r^2	0.80	0.70	0.52	0.80	0.68
smoothing and interpolation	RMSD	9	13	35	7	19
	Bias	3	−8	31	3	−18
	r^2	0.73	0.45	0.36	0.78	0.84

BGD
11, 2305–2342, 2014

Table 4. Statistics comparing remote sensing to greenness derived near-surface phenology. Statistics are computed as in Table 3. The time series method indicated in the table was used for both near-surface and remote sensing date estimates. Bias is calculated relative to near-surface estimates, so a negative bias indicates that the corresponding remote sensing estimate is later.

Remote sensing index	Time series method	Statistic	SOS	MOS	EOS	SOF	MOF	EOF
EVI	simple sigmoid	RMSD	10	6	14	28	10	24
		Bias	4	−4	−12	20	−1	−22
		r^2	0.74	0.91	0.76	0.11	0.51	0.74
	greendown sigmoid	RMSD	9	7	17	21	11	18
		Bias	4	−5	−14	10	−3	−15
		r^2	0.76	0.91	0.73	0.20	0.58	0.65
	generalized sigmoid	RMSD	9	6	12	14	10	11
		Bias	1	−3	−9	−6	−7	−8
		r^2	0.67	0.88	0.68	0.32	0.72	0.77
	smoothing and interpolation	RMSD	8	6	13			
		Bias	0	−4	−10			
		r^2	0.72	0.90	0.65			
NDVI	simple sigmoid	RMSD	18	7	12	21	17	27
		Bias	9	1	−6	−3	−3	−3
		r^2	0.41	0.82	0.71	0.18	0.27	0.11
	greendown sigmoid	RMSD	7	6	15	19	10	19
		Bias	1	0	−2	3	−6	−15
		r^2	0.81	0.83	0.47	0.23	0.76	0.67
	generalized sigmoid	RMSD	13	10	13	15	11	12
		Bias	0	−1	−3	−7	−7	−6
		r^2	0.31	0.54	0.43	0.30	0.70	0.67
	smoothing and interpolation	RMSD	12	6	12			
		Bias	5	0	−7			
		r^2	0.49	0.81	0.56			

BGD
11, 2305–2342, 2014

Table 5. Statistics comparing remote sensing to redness derived near-surface phenology. Statistics are reported as in Table 4. Smoothing and interpolation was used to estimate dates from near-surface redness time series, while the time series method indicated in the table refers to analysis of remote sensing indices.

Remote sensing index	Time series method	Statistic	SOF	MOF	EOF
EVI	simple sigmoid	RMSD	50	13	23
		Bias	48	10	−22
		r^2	0.03	0.69	0.60
	greendown sigmoid	RMSD	31	9	18
		Bias	28	5	−16
		r^2	0.29	0.70	0.57
	generalized sigmoid	RMSD	23	7	17
		Bias	21	2	−15
		r^2	0.50	0.74	0.61
NDVI	simple sigmoid	RMSD	27	10	13
		Bias	23	6	−9
		r^2	0.23	0.66	0.51
	greendown sigmoid	RMSD	25	7	20
		Bias	21	1	−15
		r^2	0.37	0.72	0.33
	generalized sigmoid	RMSD	25	7	16
		Bias	22	3	−12
		r^2	0.42	0.77	0.53

BGD
11, 2305–2342, 2014

Table 6. Statistics comparing the MEASURES phenology product to near-surface imagery. Statistics computed as in Table 4.

Time series method	Statistic	SOS	MOS	EOS	SOF	MOF	EOF
simple sigmoid	RMSD	19	16	25	32	19	20
	Bias	1	−9	−19	16	5	−5
	r^2	0.29	0.36	0.20	0.01	0.05	0.18
greendown sigmoid	RMSD	19	16	24	39	20	21
	Bias	1	−8	−18	27	10	−8
	r^2	0.28	0.36	0.21	0.00	0.06	0.24
generalized sigmoid	RMSD	19	17	23	31	19	20
	Bias	−2	−9	−15	17	8	−3
	r^2	0.26	0.30	0.11	0.00	0.07	0.23

BGD
11, 2305–2342, 2014

Table 7. Statistics comparing the MODIS phenology product to near-surface imagery. Statistics computed as in Table 4.

Time series method	Statistic	SOS	EOS	SOF	EOF
simple sigmoid	RMSD	17	28	55	16
	Bias	11	−22	50	−10
	r^2	0.37	0.30	0.01	0.53
greendown sigmoid	RMSD	17	25	65	16
	Bias	12	−19	60	−12
	r^2	0.39	0.33	0.00	0.52
generalized sigmoid	RMSD	16	25	52	13
	Bias	8	−18	48	−6
	r^2	0.23	0.22	0.02	0.57

BGD
11, 2305–2342, 2014

Study sites:
A: Acadia National Park, Maine
B: Arbutus Lake, New York
C: Bartlett Experimental Forest, New Hampshire (2 cameras)
D: Boundary Waters Canoe Area Wilderness, Minnesota
E: Dolly Sods Wilderness, West Virginia
F: Great Smoky Mountains National Park, Tennessee
G: Groundhog, Ontario
H: Harvard Forest, Massachusetts
I: Mammoth Cave National Park, Kentucky
J: Mount Vernon Trail, Washington, DC
K: Queens Biological Station, Ontario
L: University of Michigan Biological Station
M: Upper Buffalo Wilderness, Arkansas

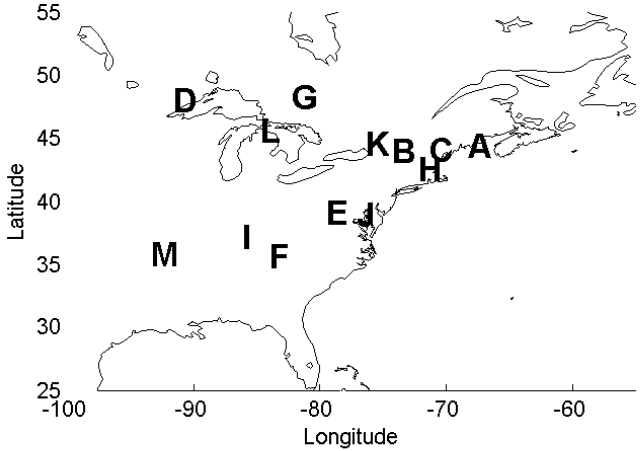

Fig. 1. Study sites.

BGD
11, 2305–2342, 2014

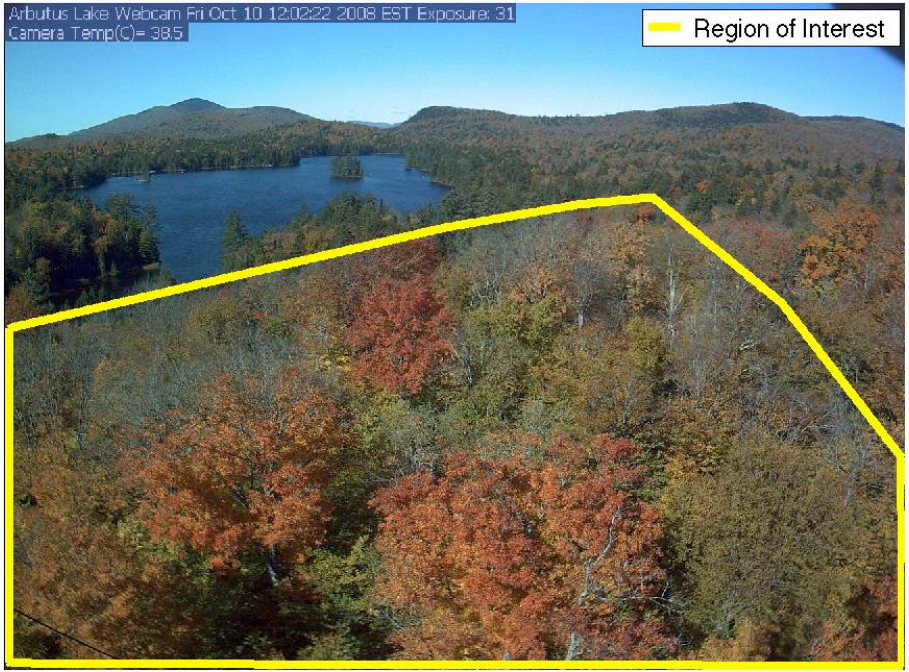

Fig. 2. ROI shown on canopy image for Arbutus Lake in New York.

BGD
11, 2305–2342, 2014

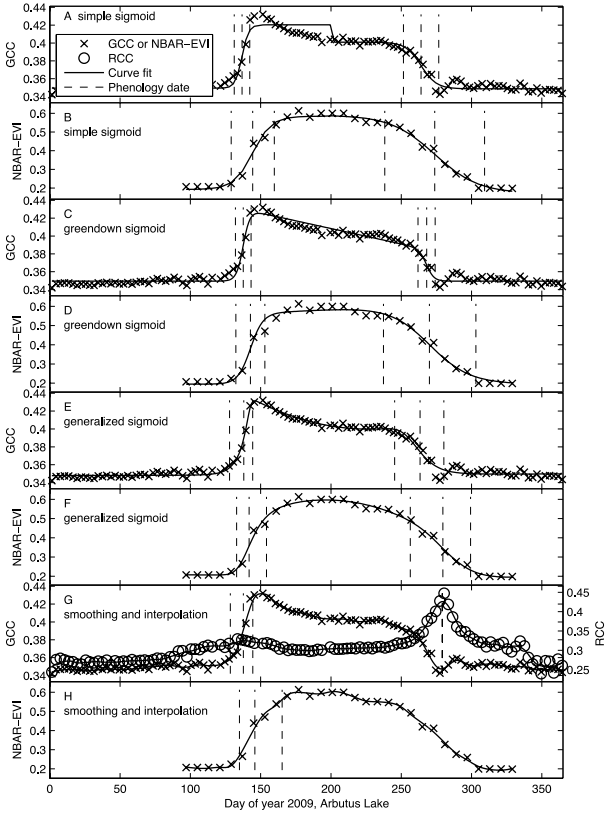

Fig. 3. Example comparison of the simple sigmoid, greendown sigmoid, generalized sigmoid, and smoothing and interpolation approaches for one year of GCC and NBAR-EVI data. Phenology date estimates represent start of spring, middle of spring, and end of spring. The simple sigmoid, greendown sigmoid, and generalized sigmoid models also have start of fall, middle of fall, and end of fall. A single autumn phenology date is identified from RCC using the smoothing and interpolation model.

BGD
11, 2305–2342, 2014

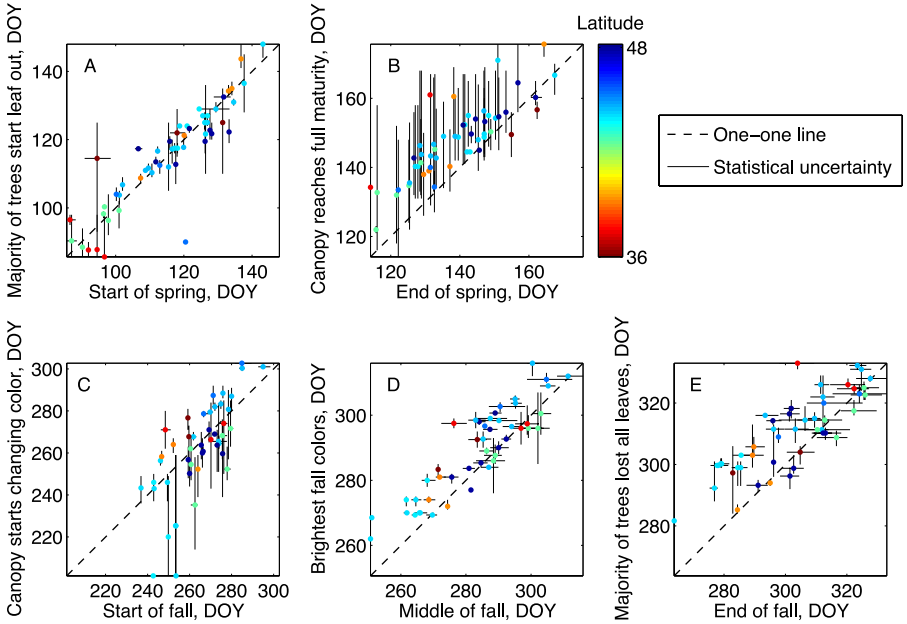

Fig. 4. Scatter plots of the comparison between visually assessed dates (y-axis) and dates identified from near surface GCC (x-axis) using the generalized sigmoid method.

BGD
11, 2305–2342, 2014

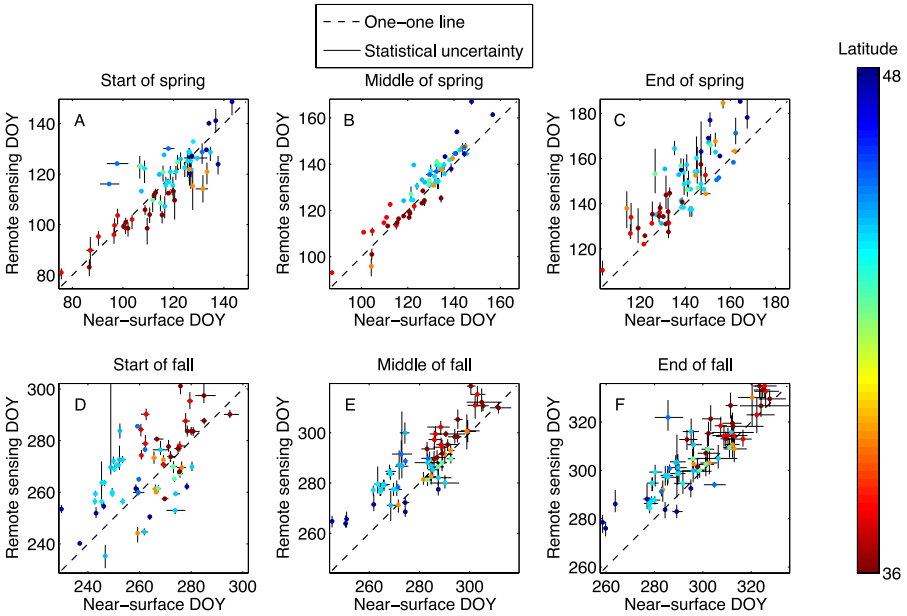

Fig. 5. Scatter plots of the comparison between near surface GCC analysis and remote sensing of NBAR-EVI using the generalized sigmoid method.

BGD
11, 2305–2342, 2014

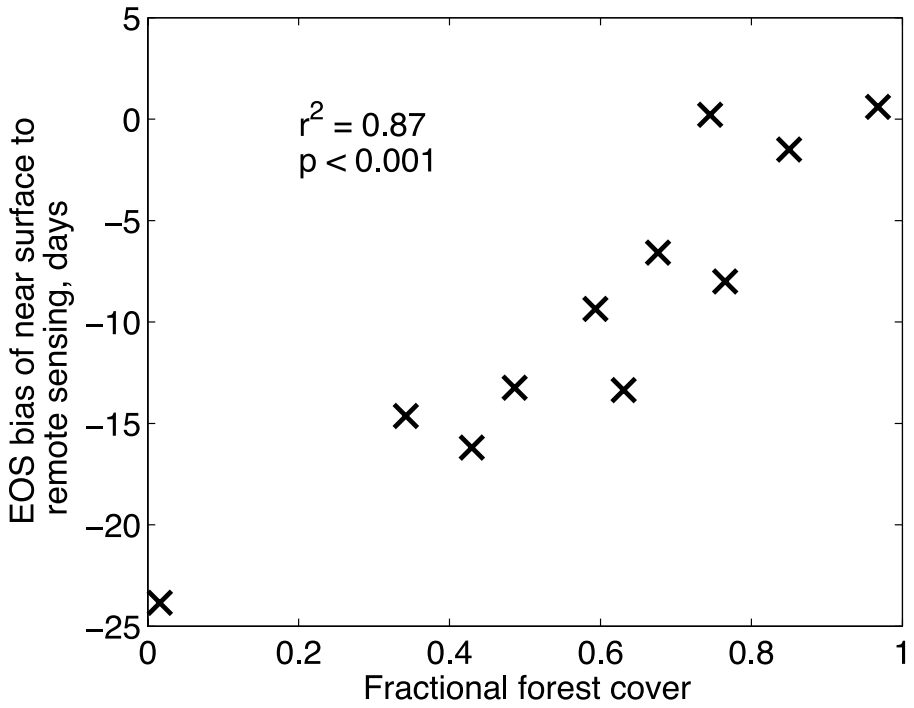

Fig. 6. Scatter plot of bias in the end of spring (EOS) between near surface GCC date estimates and remote sensing NBAR-EVI estimates using the generalized sigmoid method, for sites located in the US. Fractional forest cover is defined as the fraction of NLCD pixels in the deciduous or mixed forest classes at each study site.

BGD
11, 2305–2342, 2014